Thermodynamic product retrieval methodology and validation for NAST-I

Daniel K. Zhou, William L. Smith, Jun Li, Hugh B. Howell, Greg W. Cantwell, Allen M. Larar, Robert O. Knuteson, David C. Tobin, Henry E. Revercomb, and Stephen A. Mango

The National Polar-Orbiting Operational Environmental Satellite System (NPOESS) Airborne Sounder Testbed (NAST) consists of two passive collocated cross-track scanning instruments, an infrared interferometer (NAST-I) and a microwave radiometer (NAST-M), that fly onboard high-altitude aircraft such as the NASA ER-2 at an altitude near 20 km. NAST-I provides relatively high spectral resolution (0.25-cm^{-1}) measurements in the 645–2700-cm^{-1} spectral region with moderate spatial resolution (a linear resolution equal to 13% of the aircraft altitude at nadir) cross-track scanning. We report the methodology for retrieval of atmospheric temperature and composition profiles from NAST-I radiance spectra. The profiles were determined by use of a statistical eigenvector regression algorithm and improved, as needed, by use of a nonlinear physical retrieval algorithm. Several field campaigns conducted under varied meteorological conditions have provided the data needed to verify the accuracy of the spectral radiance, the retrieval algorithm, and the scanning capabilities of this instrumentation. Retrieval examples are presented to demonstrate the ability to reveal fine-scale horizontal features with relatively high vertical resolution.

OCIS codes: 010.0010, 010.1280, 280.0280.

1. Introduction

Temperature and water vapor are basic meteorological parameters for weather forecasting. In addition, they are critical parameters in tropospheric chemistry studies. Observation from an infrared Fourier transform spectrometer (FTS) flown on an aircraft, or a spacecraft, can be used to infer the atmospheric temperature, moisture, and the concentration of other chemical species by use of radiative transfer equation inversion techniques.[1–3] The National Polar-Orbiting Operational Environmental Satellite System (NPOESS) Airborne Sounder Testbed (NAST) has been successfully operating on high-altitude aircraft (ER-2 and Proteus) since 1998.[4,5] NAST-I was designed to provide radiometric measurements similar to those to be obtained from future satellite sensors such as the Atmospheric Infrared Sounder (AIRS) on the Aqua (2002), the Geosynchronous Imaging Fourier Transform Spectrometer (GIFTS) on the EO-3 (2005), the Interferometer Atmospheric Sounding Instrument (IASI) on the Meteorological Operational (METOP) (2005), and the Cross-track Infrared Sounder (CrIS) on the NPP (2006) and the NPOESS (2008) satellites.

A fast and accurate inversion algorithm becomes critical when one deals with high-spatial and hyperspectral resolution remote-sounding data. Detailed and accurate analyses of NAST-I data, by use of linear regression of radiance eigenvector amplitudes against atmospheric state variables[2] with an accurate fast transmittance model[6,7] and NAST-I measurements, have demonstrated that fast and accurate retrieval of temperature and moisture profiles can be achieved.[8] An ozone regression retrieval, achieved simultaneously with temperature and moisture, has also been performed.[9] The same regression methodology has been applied to NAST-I and NAST-M data in combination, thereby providing an all-weather sounding capability. NAST-I has provided hyperspectral resolution remote-sensing data, which provides independent validation, from many field

D. K. Zhou (d.k.zhou@larc.nasa.gov), W. L. Smith, and A. M. Larar are with Atmospheric Science Competency, NASA Langley Research Center, Hampton, Virginia 23681. J. Li, H. B. Howell, R. O. Knuteson, D. C. Tobin, and H. E. Revercomb are with the Space Science and Engineering Center, University of Wisconsin–Madison, Madison, Wisconsin 53706. G. W. Cantwell is with the Space Dynamics Laboratory, Utah State University, Logan, Utah 84341. S. A. Mango is with the National Polar-Orbiting Operational Environmental Satellite System Integrated Program Office, 8455 Colesville Road, Silver Spring, Maryland 20910.

Received 22 January 2002; revised manuscript received 2 July 2002.

0003-6935/02/336957-11$15.00/0

campaigns. Samples of NAST-I geophysical products (e.g., distributions of temperature, moisture, surface skin temperature) obtained during these validation campaigns are presented herein, along with a description of the profile retrieval methodology (regression and physical iteration) that was used to achieve the results.

2. Experiments and Observations

NAST-I instrumentation, measurements, calibration, and radiance validation are documented elsewhere.[4,10,11] NAST-I measured radiance spectra cover CO_2 emission within the 15- and 4.3-μm bands, H_2O emission across the 6.3-μm band, O_3 emission within the 9.6- and 4.7-μm bands, and CO emission within the 4.6-μm band. These radiance measurements can be used to retrieve temperature, water vapor, ozone, and carbon monoxide profiles. Even though a large amount of data have been collected since July 1998 under a variety of meteorological conditions, results from only a limited data set are needed and presented in this paper for the purpose of retrieval algorithm validation. A more complete overview of results from the numerous field campaigns in which the NAST has collected data is in preparation. Retrievals from the Convection and Moisture Experiment 3 (CAMEX-3) Atlantic basin tropical cyclone field validation NASA ER-2 flight (during local nighttime, 13–14 September 1998) over Andros Island, Bahamas, are presented here. These, together with the radiosonde and ground-based remote-sensing observations (e.g., Raman lidar) made from Andros Island, provide a unique data set for detailed analysis of retrieval resolution and accuracy. During this particular calibration–validation flight, water vapor measurements were also provided by the Lidar Atmospheric Sensing Experiment (LASE) onboard the NASA DC-8 aircraft[12] flow below the NASA ER-2 aircraft. All coincident observations obtained during this experiment are used to understand the atmospheric state for validating NAST-I retrievals of temperature and water vapor.

The retrievals obtained from cloudy regions will contain intolerable error near and below the cloud level if the attenuation of infrared radiation emitted from the Earth's surface and the atmosphere below the cloud are not properly accounted for in the retrieval process. Cloud-cleared radiances[13] in cloudy regions were used for the analyses and retrieval processing presented in this paper. NAST-I measured radiances were classified as either clear or nonclear as described in the following empirical manner. NAST-I measurements were classified as clear if the following three criteria were met: $|T_{11} - T_{10}| \leq 2$ K, $|T_{12} - T_{11}| \leq 2$ K, and $T_w \geq 294$ K, where T_{10}, T_{11}, T_{12}, and T_w are the brightness temperatures at 10-, 11-, and 12-, and the window region (893.7–903.8 cm^{-1}), respectively; otherwise, the measurement was classified as nonclear. Each of the nonclear measurements was cloud cleared by the methodology initially presented by Smith.[14] This method assumes that the only difference in the measured radiance between adjacent measurements is the amount of cloud cover in each of the scenes. Using pairs of adjacent measurements, at least one of which is a cloudy measurement and a simultaneous clear measurement in a spectral window region, we could calculate estimates of the clear column radiance for measurements made over cloudy regions. It is assumed that the surface radiance as observed in the window spectral channel is also representative of clouded columns, a good assumption over oceanic regions. Detailed studies of cloud-clearing accuracy versus field-of-view size performed by use of NAST-I data reveal rapid degradation with an increase in field-of-view size.[13] The fact that NAST-I measurements have moderate spatial resolution and broad infrared regional coverage allows cloud clearing to be performed with a highly achievable degree of accuracy when applied at the full spatial resolution of the NAST interferometer.

3. Linear Regression Methodology and Analyses

Atmospheric temperature, moisture, and surface property retrieval from near-nadir-viewing spectral radiances is accomplished in two steps: (1) regression retrieval obtained by use of a linear statistical regression of radiance eigenvector amplitudes against atmospheric state parameters based on a historical radiosonde training database and (2) physical retrieval achieved by use of the eigenvector regression results as the first guess by iteration of the radiative transfer calculations to achieve a solution that best fits the radiance observations. Since the retrieval problem described is ill-posed, additional information is needed to constrain the solution. Here, radiosonde sample statistics constrain the regression algorithm and the results can be used as the initial or first-guess profile to constrain the physical retrieval. The linear statistical eigenvector regression retrieval provides first-guess profiles and surface properties that minimize the number of iterations and computation time required for physical retrieval processing.

A. Linear Statistical Regression

The basic linear statistical regression theory is now summarized. Given a set of historical radiosonde measurements and associated simulated spectral radiance R, the relationship between an atmospheric state and associated radiances is expressed statistically in terms of regression coefficients. R is calculated from the radiosonde atmospheric state and assumed surface properties $A(T, Q, T_s, \varepsilon_s)$, where T is the temperature profile, Q is the water vapor profile, T_s is the surface temperature, and ε_s is the surface emissivity. The surface emissivity spectrum for each radiosonde profile is randomly selected from a set of laboratory measured emissivity spectra for a

wide variety of surface types.[15] Using amplitudes of statistical eigenvectors of radiance as the predictors filters the radiance noise and effectively stabilizes the retrieval.[2] Eigenvectors E [i.e., empirical orthogonal functions, (EOFs)] can be generated by use of the covariance matrix M from a set of radiances associated with a radiosonde training data set (total number of S profiles and number of selected spectral channels denoted by nc). This covariance matrix is expressed as

$$M_{ij} = \frac{1}{S}\sum_{k=1}^{S} \mathcal{R}_{ki}\mathcal{R}_{kj}, \tag{1}$$

where $\mathcal{R}_{kj}$ is the radiance (deviation from the sample mean) at spectral position j of sample k. We define the eigenvector matrix U by resorting to the singular-value decomposition of covariance matrix M. The eigenvectors that comprise matrix U in Eq. (1) are ordered from the largest amount of variance to the residual variance in successively decreasing order. The elements of the radiance eigenvector amplitude vector C (i.e., the radiance predictor in the eigenvector domain) is given by

$$C_i = \sum_{j=1}^{nc} \mathcal{R}_j U_{ji}. \tag{2}$$

The statistical regression coefficient matrix K derived from a set of radiosonde observations provides the matrix relationship between the surface and the atmospheric variables A, and associated radiance vector $\mathcal{R}$ and surface pressure P_s:

$$\begin{aligned} A_j &= \sum_{i=1}^{n-1} K_{ji}C_i + K_{jn}P_s \\ &= \sum_{i=1}^{n-1} K_{ji}\left(\sum_{l=1}^{nc} \mathcal{R}_l U_{li}\right) + K_{jn}P_s, \end{aligned} \tag{3}$$

where n is the number of EOFs (i.e., the number of principal components used for the regression retrieval). The surface emissivity can also be retrieved by prediction of the amplitudes of a small set of emissivity eigenvectors used to represent the laboratory sample of emissivity spectra utilized for the radiance simulations.[16]

NAST-I contains a scanning mirror that allows the viewing angle to vary from −45 to +45 deg with a step of 7.5 deg in the cross-track direction. The zenith angle is associated with the viewing angle and aircraft roll angle at each NAST-I scan position. The regression coefficients are derived for a fixed set of zenith angles while the retrieval for a specific zenith angle of a scan is obtained by linear interpolation of the two retrievals obtained by use of regression coefficients for the two closest zenith angles. Regression coefficients are defined for as many angles as necessary to account correctly for radiance dependence on zenith angle in the retrieval process.

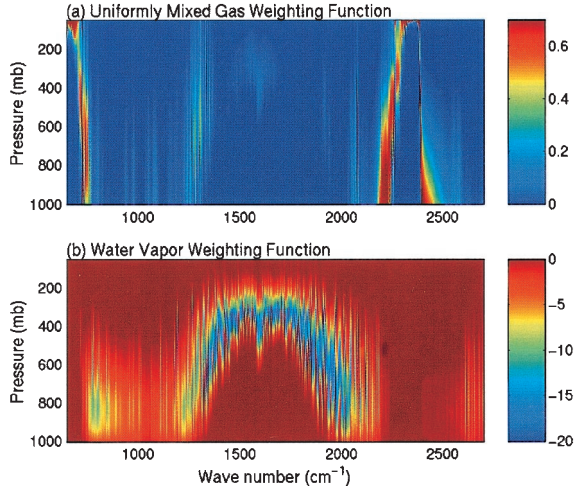

Fig. 1. Weighting function matrices of (a) fixed gas (constant mixing ratio) and (b) water vapor of NAST-I channels calculated with the U.S. 1976 Standard Atmosphere. The peak (or valley) of the weighting function of fixed gas (or water vapor) of each channel indicated in wave number is associated with a pressure altitude.

B. Training Data, Analyses Approach, and Optimal Regression

The analyses presented here use the case from CAMEX-3 described in Section 2. The CAMEX-3 radiosonde training profiles were taken from August to September 1997. Radiosonde station latitudes were from 17 °N to 40 °N and longitudes were from 75 °W to 94 °W for a total of 29 stations and 3188 radiosondes. We synthetically produced the associated ozone profiles using the regression statistics derived from the NASA Wallops Flight Facility (WFF) ozonesonde database collected between July 1995 and March 2000.[17]

NAST-I possesses three spectral bands that together provide 8632 spectral channels. To limit the size of EOFs that accommodate the computer memory requirements for EOF computation, we chose spectral segments to contain channels that provide the most information about temperature, water vapor, ozone, carbon monoxide, and surface properties as required for accurate regression statistics. These spectral segments were selected on the basis of the retrieval sensitivity to the spectral radiances, which is illustrated by the weighting function (or Jacobian) matrix. Weighting functions can be calculated by an analytical scheme or a numerical perturbation method.[18,19] Examples shown in Fig. 1 are the weighting function matrices for gases of constant mixing ratios (e.g., CO_2 and N_2O) and for water vapor (H_2O) simulated for NAST-I by use of the U.S. 1976 Standard Atmosphere. It is noted that the weighting functions associated with constant mixing ratio gases and water vapor have peaks distributed throughout the range of pressure altitude. In other words, the channels in these spectral regions can be used for temperature and water vapor profile retrieval. These weighting functions are also used to select the channels for the physical retrieval to be discussed in

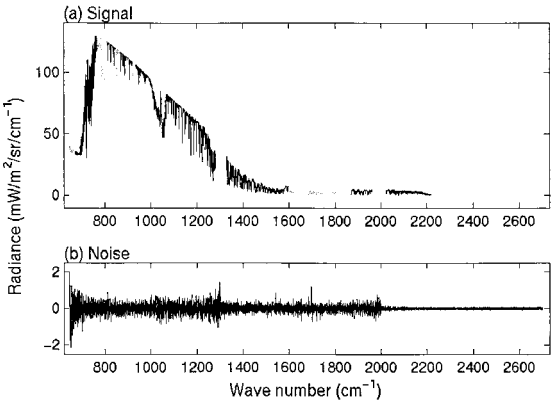

Fig. 2. (a) Simulated NAST-I spectral radiance from the radiosonde collected on Andros Island, Bahamas (24.7 °N, 77.8 °W) at 00:30 UTC, 14 September 1998. The channels indicated in black were selected for regression analyses and retrieval. (b) Estimated NAST-I random noise level for this flight as obtained from calibration blackbody looks.

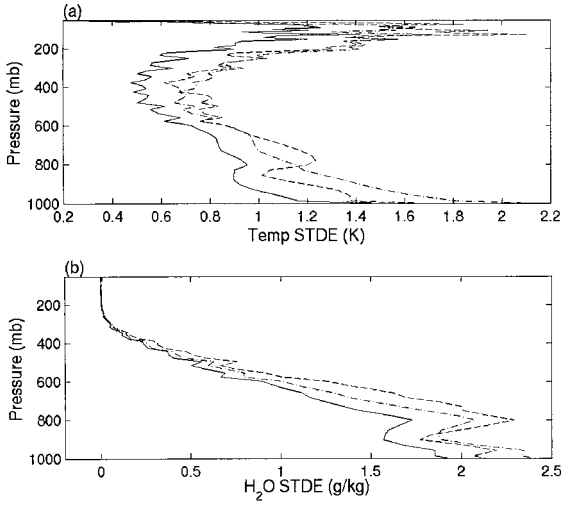

Fig. 3. STDE over dependent samples (CAMEX-3 training data set) as a function of the number of EOFs for (a) temperature and (b) water vapor assuming NAST-I calibration noise (EOF numbers of 10, 26, and 58 are indicated by dash–dot, solid, and dashed curves, respectively).

Section 4. The selected spectral segments for regression analyses and retrieval are indicated in Fig. 2(a) (black regions), which also shows a simulated NAST-I spectrum (from the ER-2 altitude of ~20 km) and a spectrum of instrument noise. NAST-I spectral channels totaling 4514 were selected and used in the regression retrieval analysis.

Fundamental questions must be considered to achieve the optimal regression solution. (1) How many principal components (i.e., EOFs) are appropriate to produce the optimal regression retrieval? (2) How does the noise (i.e., instrument noise and forward model error) affect the optimal number of EOFs? Two methods are investigated to estimate the optimal number of EOFs for retrieval: (1) a model simulation method with the knowledge of NAST-I noise level and (2) a NAST-I measured and retrieval-simulated radiance fitting method performed without knowledge of the measurement noise level. Both methods define the optimal number of EOFs for processing the NAST-I measurements.

The advantage of radiative transfer model simulation of NAST-I observed radiances is that the truth profile (i.e., the radiosonde observation) is known and the retrieval can be directly compared with the truth to define an optimal EOF number. However, this approach requires an accurate representation of the total system noise level. The standard deviations of the regression error (STDE) differences between the truth and the retrieval for the dependent sample (the training database for the CAMEX-3 data set) are shown in Figs. 3(a) and 3(b) for temperature and water vapor, respectively. The vertical mean of the STDE is also shown in Figs. 4(a) and 4(b). From this typical case, the optimal EOF number (associated with minimal error) for simultaneous temperature and water vapor retrieval can be defined if the total noise is the NAST-I radiometric noise observed during calibration of the instrument. The same analysis has been conducted with the noise reduced by 50% to illustrate how an optimal EOF number and retrieval accuracy are affected by the instrument noise level. The optimal number of EOFs, as expected, is increased and the retrieval error is reduced [see Figs. 4(a) and 4(b)]. This indicates the importance of specifying the noise accurately since the retrieval accuracy depends on the optimal EOF number. Similar results are obtained from an independent sample of radiosonde cases.

The least-squares fitting of retrieval-simulated radiances to actual radiance observations is used to define the optimal EOF number that accounts for forward model error as well as the actual measurement noise. A set of observed spectral radiances (under cloud-free conditions) and spectral radiances simulated from the associated retrievals can be com-

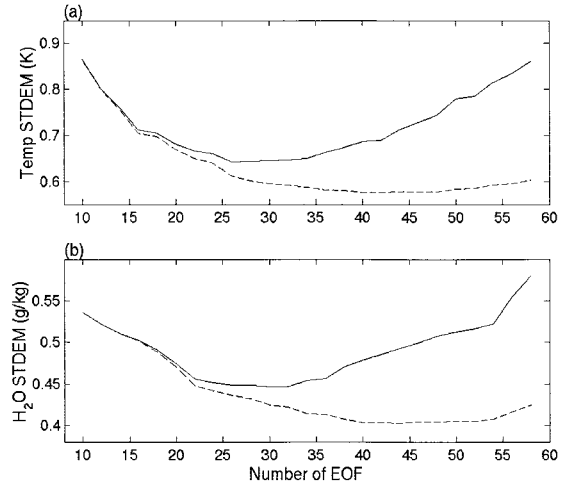

Fig. 4. Mean of profile STDE for (a) temperature and (b) water vapor shown as solid (full NAST-I calibration noise) and dashed curves (half NAST-I calibration noise).

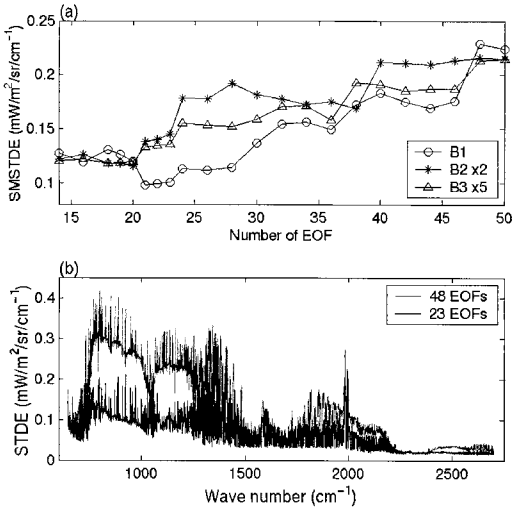

Fig. 5. Standard deviation of radiance difference between observed and retrieval simulated (see text) as a function of the number of EOFs: (a) band sample mean [note: band 1 (645–1300 cm^{-1}), band 2 (1290–1999 cm^{-1}), band 3 (1985–2700 cm^{-1}) are multiplied by 1, 2, and 5, respectively] and (b) spectral distribution.

pared to find the minimum standard deviation of the differences through the spectral radiance domain that corresponds to the EOF number. NAST-I data collected over Andros Island (13–14 September 1998) within the latitudes of 24.6° and 24.8 °N, the longitudes of 77.7° and 77.9 °W, and viewing angles of less than 20° (a total of 118 single scans) were used to define the optimal EOF number. These observations were selected near the radiosonde site for retrieval validation purposes. The standard deviations of the spectral radiance differences between observations and simulations from retrievals associated with the same observations are shown in Fig. 5 as a function of the number of EOFs [only two curves are plotted in Fig. 5(b) for clarity]. The optimal EOF number is defined as the number that provides the best fit of the calculated radiance spectrum to the observed radiance spectrum; this is achieved without *a priori* knowledge of a specific noise level.

In this case, we derived the comparable optimal EOF number by using two approaches (i.e., 26 from the simulation method and 23 from the observation method), revealing that accurate noise estimation is obtained from the calibration data. However, the forward model error was not accounted for in the model simulation method (Figs. 3 and 4); therefore, the optimal EOF number derived from observations is expected to be smaller than that defined as pure simulation analyses. When the number of EOFs is larger (or smaller) than the optimal, the effect of noise is not optimally minimized (or part of the atmospheric content is filtered out and the vertical resolution is reduced). It is clear that an accurate regression depends on an optimal EOF number that will minimize the effect of noise and produce optimal sensitivity. It is noteworthy that the optimal number of EOFs also depends on the training data set and the channel selection. An optimal number of EOFs can be determined by one of the two methods illustrated above. The optimal EOF number minimizes the retrieval error and optimizes the vertical resolution achievable for the noise level. Field campaigns with varied meteorological conditions have provided the data needed to verify the accuracy of NAST-I spectral radiance, including the forward model, the retrieval algorithm, and the capabilities of this instrument. These same analyses have been performed over many different training data sets for varied meteorological conditions, leading us to conclude that NAST-I optimal regression achieves an accuracy for a temperature of ~1.0 deg rms and water vapor of ~20% rms for 1- and 2-km layers, respectively.

C. Regression Validation

NAST-I has successfully collected high-quality data throughout many field campaigns. A sample of regression retrievals is presented here to demonstrate the nadir temperature and water vapor profiling regression. There were five radiosondes launched during the period from 22:30 UTC, 13 September, to 02:40 UTC, 14 September 1998 from the same location of latitude 24.7 °N and longitude 77.8 °W (Andros Island, Bahamas). NAST was onboard the ER-2 and flown over the radiosonde site to provide the data needed for NAST-I retrieval algorithm validation. Two sets of regression retrievals, resulting from the 26 and the 23 EOFs, are presented here for comparison. The mean of these radiosondes was plotted in Figs. 6(e) (temperature) and 6(f) (relative humidity) for comparison with the spatially averaged NAST-I temperature [Figs. 6(a) and 6(b)] and relative humidity [Figs. 6(c) and 6(d)] retrievals, respectively. The segment for which the spatial averaging is performed is closest in time and location to the radiosonde observation. It is noteworthy that this retrieval depends solely on the observed radiances (i.e., there was no tuning based on radiosonde data) and is within the accuracy expectation. The atmospheric state was retrieved to simulate NAST-I spectral radiances, which were then compared with the associated NAST-I observed radiances to illustrate the accuracy of this regression. This spectral radiance validation has shown minimized discrepancy similar to the results (with 26 EOFs) in Fig. 5.

4. Physical Retrieval Algorithm

NAST-I has 8632 spectral channels to provide abundant information on atmospheric parameters; even though many channels are redundant in spectral information, they are independent in terms of random measurement noise. Thus, as many channels as possible should be used for the statistical retrieval processing but a subset of optimal channels was selected for subsequent physical retrieval. The optimal channels for which the spectroscopy is well known should provide nonredundant information for both temperature and atmospheric constituents; in addition, they are those that have small detector

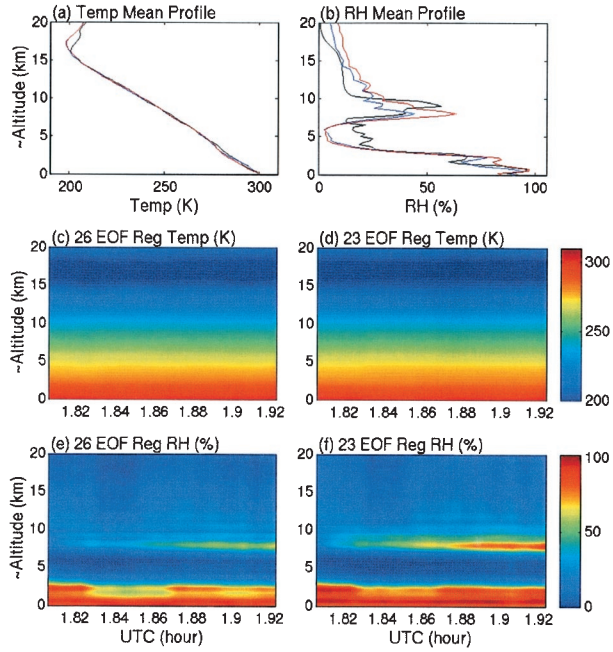

Fig. 6. Sample of NAST-I regression and radiosonde comparison from CAMEX-3 validation flight over Andros Island, Bahamas, 14 September 1998. Radiosonde profile (black) and NAST-I means from 26 (blue) and 23 (red) EOF regressions plotted in (a) and (b) for temperature and relative humidity, respectively. The cross sections of temperature and relative humidity resulting from 26 and 23 EOF regressions are shown. The ER-2 flew over the radiosonde site at ~1.82 UTC. The aircraft location (latitude and longitude) associated with UTC is indicated in Fig. 12.

noise and a small calibration error. These channels are desired in-between line centers, since here the sharpest weighting functions occur. To use the same eigenvectors used in the regression processing to reconstruct (i.e., to reduce the noise of) NAST-I radiances for physical retrieval, these optimal channels are selected in the same spectral regions (indicated in Fig. 2) used for the regression retrieval. The selected optimal channels for physical retrieval are shown in Fig. 7 along with a NAST-I brightness temperature spectrum.

Once the first guess is generated from the regression technique described above, a nonlinear iterative

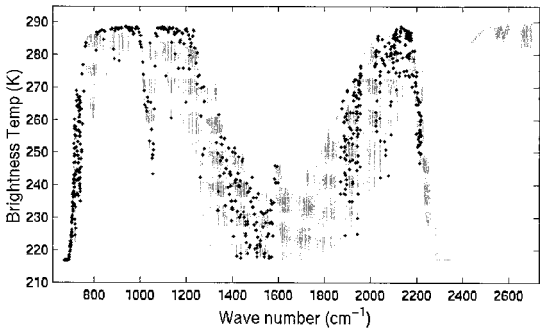

Fig. 7. NAST-I brightness temperatures and selected optimal channel index (in dots) used in the physical retrieval processing.

procedure is set up to produce a retrieval that is an improvement of the first guess (i.e., the regression retrieval). Here, the upwelling spectral radiances are represented by the radiative transfer equation (excluding any scattering and reflection):

$$R - R^s = \varepsilon B_s \tau_s - \int_{P_{ac}}^{P_s} B d\tau + (1 - \varepsilon) \int_{P_{ac}}^{P_s} B d\tau^*, \quad (4)$$

where $\tau^* = \tau_s^2/\tau$; R is the spectral radiance at a certain frequency; R^s represents the contribution of reflected solar radiation in the infrared region and can be eliminated for channels with a wavelength longer than 4.0 μm in daytime, ε refers to the Earth's surface emissivity; $B[\nu, T(p)]$ is the Planck function at wave number ν and at temperature $T(p)$; p is the pressure; τ is the atmospheric transmittance from any given level to the top of the atmosphere (or the sensor); P_{ac} is the aircraft pressure; and P_s is the surface pressure (subscript s denoting surface). A fast model[6,7] with vertical pressure coordinates from 50 to 1100 hPa (or millibars) is used for the NAST-I transmittance calculation. The pressure grid is established according to $p(i) = (a \times i^2 + b \times i + c)^{7/2}$, where we determined parameters a, b, and c by solving the equation of $p(1) = 1100$ mbars, $p(38) = 300$ mbars, and $p(101) = 5 \times 10^{-3}$ mbars.

If the NAST-I observed radiance R_ν^m of each channel is known, then R_ν^m can be considered a nonlinear function of the atmospheric temperature profile, water vapor mixing ratio profile, ozone mixing ratio profile, surface skin temperature, surface emissivity, etc. That is, $R_\nu^m = R_\nu(T, Q, T_s, \varepsilon, \ldots) + \sigma_\nu$ (σ_ν is the instrument noise and other sources of error). In general,

$$Y^m = Y(X) + \sigma, \quad (5)$$

where the state vector X contains atmospheric temperatures (L levels of atmosphere), atmospheric moisture mixing ratios (the moisture is expressed as the logarithm of the mixing ratio in practical applications), one surface skin temperature, etc. and Y^m contains N (number of channels used) observed radiances. The linear form of Eq. (5) is

$$\delta Y = Y' \delta X, \quad (6)$$

where Y' is the linear tangent of the forward model Y, the weighting function (or Jacobian) matrix. These weighting functions can be calculated by a differential scheme or perturbation method. However, an accurate and efficient analytical way to calculate the weighting functions is important for real-time advanced sounder data retrieval processing. Here the linear model Y' uses an efficient analytical form.[18,20] A general form of the minimum variance solution minimizes the following penalty function[21]:

$$J(X) = [Y^m - Y(X)]^T E^{-1} [Y^m - Y(X)] + [X - X_0]^T H [X - X_0], \quad (7)$$

where superscript T denotes the transpose. By using the Newtonian iteration,

$$X_{n+1} = X_n + J''(X_n)^{-1}J'(X_n), \tag{8}$$

the following quasi-nonlinear iterative form[22] is obtained:

$$\delta X_{n+1} = ({Y'_n}^T E^{-1} Y'_n + H)^{-1} {Y'_n}^T E^{-1}(\delta Y_n + Y'_n \delta X_n), \tag{9}$$

where $\delta X_n = X_n - X_0$, $\delta Y_n = Y^m - Y(X_n)$, X is the atmospheric profile to be retrieved, X_0 is the initial state of the atmospheric profile or the first guess, Y^m is the vector of the observed radiances or brightness temperatures used in the retrieval process, E is the observation error covariance matrix that includes instrument noise and forward model error, and H is the *a priori* matrix that constrains the solution. H can be the inverse of the *a priori* first-guess error covariance matrix or another type of matrix. If the statistics of both the measurement and *a priori* error covariance matrix are Gaussian, then the maximum-likelihood solution is obtained. However, if the *a priori* error covariance matrix is not known or is estimated incorrectly, the solution will be suboptimal.[7] Here we let $H = \gamma I$ in Eq. (9), where γ is a Lagrangian multiplier that serves as a smoothing factor. Equation (9) becomes

$$\delta X_{n+1} = ({Y'_n}^T E^{-1} Y'_n + \gamma I)^{-1} {Y'_n}^T E^{-1}(\delta Y_n + Y'_n \delta X_n), \tag{10}$$

which is commonly referred to as the minimum information solution. The smoothing factor γ is difficult to determine but extremely important to the solution. It is noted that γ is dependent on the observations, the observation error, and the first guess of the atmospheric profile; often it is chosen empirically.[23–25] The solution can be overconstrained and large biases can be created in the retrieval when γ is too large. The solution can be underconstrained and possibly unstable when γ is too small. In the NAST-I retrieval procedure, the discrepancy principle[26–28] is applied to determine the appropriate smoothing factor γ. Thus

$$\|Y[X(\gamma)] - Y^m\|^2 = \sigma^2, \tag{11}$$

where $\sigma^2 = \sum_{k=1}^{N} {e_k}^2$, e_k is the square root of the diagonal of E or the observation error of channel k, which includes instrument error [e.g., Fig. 2(b)] and forward model error (that is, ${e_k}^2 = {\eta_k}^2 + {f_k}^2$, where η_k is the instrument noise of channel k, whereas f_k is the forward model error that is assumed to be 0.5 K for the same channel). Usually σ^2 can be estimated from the instrument noise and the validation of the atmospheric transmittance model used in the retrieval. Since Eq. (11) has a unique solution for γ,[26] the atmospheric parameters and the smoothing factor can be determined simultaneously. In NAST-I retrieval processing, a simple numerical approach is adopted for solving Eq. (11); γ is changed in each iteration according to

$$\gamma_{n+1} = q_n \gamma_n, \tag{12}$$

where q is a factor for γ increasing or decreasing. Based on Eq. (11), q is obtained in each iteration by satisfying the following conditions:

$q_0 = 1.0$;
if $\|Y(X_n) - Y^m\| < \sigma^2$, then $q_n = 1.5$;
if $\|Y(X_n) - Y^m\| = \sigma^2$, then stop the iteration;
if $\|Y(X_n) - Y^m\| > \sigma^2$, then $q_n = 0.5$.

The q factor has been found from empirical experience to ensure that the solution is stable between iterations. Thus, γ continues to change until the iteration stops.

In the retrieval processing, several checks are made for retrieval quality control. The rms of quantity $[Y(X_i) - Y^m]$ from all selected channels χ_i is computed to check the convergence (or divergence). If $\chi_{i+1} > \chi_i$ within two iterations (i.e., iteration diverges), then the iteration is stopped and the retrieval is set to the first guess (or the previous atmospheric state); otherwise, iteration continues until $\chi_n < 1.0$ K and $|\chi_n - \chi_{n-1}| < 0.01$ K, or a maximum of ten iterations is reached. The degree of convergence of each iteration depends on the accuracy of the previous atmospheric and surface state. In addition, at each iteration, each level of the water vapor profile is checked for supersaturation. A unity magnitude of relative humidity is assumed at any supersaturated level.

5. Results, Validation, and Discussion

This physical retrieval algorithm is tested through simulations and then applied to actual NAST-I measurements. The achievement of convergence through iteration has been shown in most cases, verifying the integrity of the algorithm. To demonstrate how this physical iteration is performed, one single scan of NAST-I measurements from the 13–14 September 1998 experiment is used here as an example. Figure 8(a) shows the brightness temperature difference between the NAST-I observed and retrieval simulation. The open circles are from regression retrievals (by use of 26 EOFs) and the dots are from physical retrievals. The brightness temperature differences for these optimal channels are minimized through the physical retrieval solution. The associated temperature and moisture profile differences are plotted in Figs. 8(b) and 8(c), respectively, and show that the physical retrieval affects the final water vapor profile result more significantly than the final temperature profile result.

The same data as used for linear regression analysis are used here in physical retrieval processing to compare the first guess (i.e., the EOF regression retrieval) and the final physical retrieval. The same data set shown in Fig. 6 is again shown in Fig. 9 after

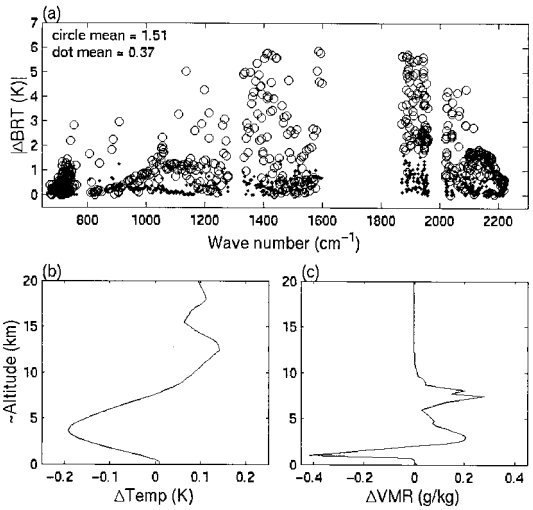

Fig. 8. Convergence example from physical iteration shows that (a) the absolute difference of brightness temperature between observed and retrieval simulations is minimized from the first guess (open circles, 26 EOF regression) to the final (physical retrieval, dots). The differences between (b) temperature and (c) moisture profiles associated with (a) radiance adjustment are indicated.

physical retrieval processing for comparison with the first guess for a relatively large section of the vertical cross sections of temperature and moisture. The final retrievals by use of the first guess of 26 and 23 EOF regressions and indication that the difference

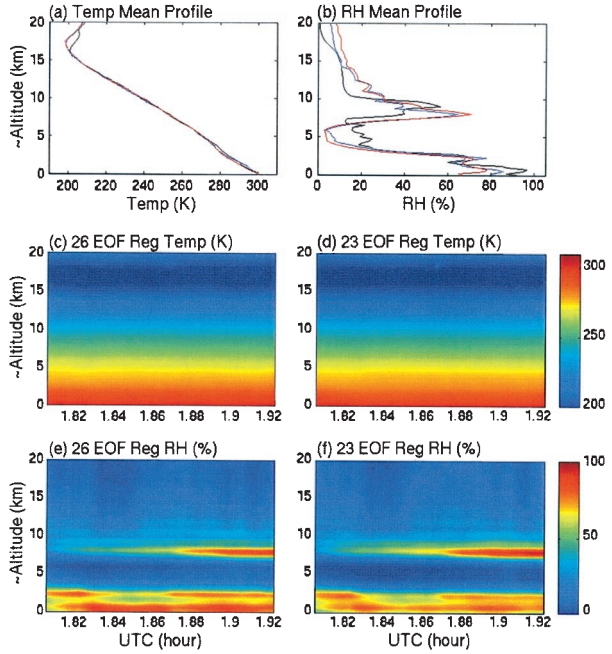

Fig. 9. Similar to Fig. 6 but physical retrievals that use regression as a first guess. Radiosonde profile (black) and NAST-I mean of physical retrievals by use of 26 (blue) and 23 (red) EOF regressions as first guesses plotted in (a) and (b) for temperature and relative humidity, respectively. Shown are the cross sections of temperature and relative humidity that resulted by use of 26 and 23 EOF regressions as first guesses (see text).

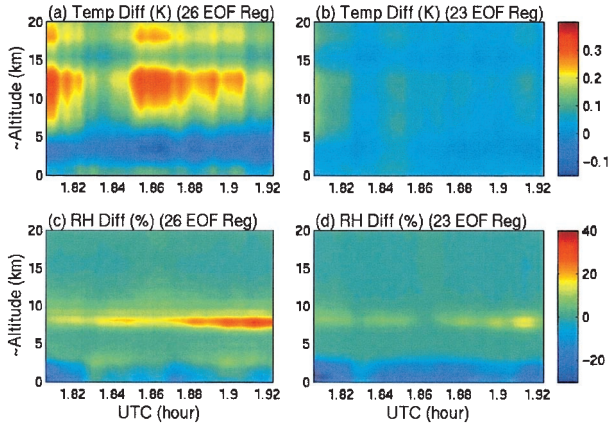

Fig. 10. Differences of (a) temperature and (c) relative humidity vertical cross sections between the physical retrieval [Figs. 9(c) and 9(e)] and the 26 EOF regression retrievals [Figs. 6(c) and 6(e)]. Differences of (b) temperature and (d) relative humidity vertical cross sections between the physical retrieval [Figs. 9(d) and 9(f)] and the 23 EOF regression retrievals [Figs. 6(d) and 6(f)].

between these two sets of retrievals is significantly minimized after the physical processing in comparison with the initial regressions shown in Fig. 6 are shown in Fig. 9. The difference between the regression and the physical retrieval, or Fig. 6 and Fig. 9, is shown in Fig. 10. The degree of excellence for the regression retrieval is also apparent from the fact that the physical iterative retrieval did not alter it significantly when used as the first guess. In most cases, the regression retrieval is only slightly modified after the physical retrieval processing. A significantly large amount of computation time is required by this physical retrieval even though the first guess is close to the conclusion. The difference in the regression retrieval and the physical retrieval of this data set, shown in Fig. 10, indicates that the dissimilarities are small except for those of water vapor within narrow layers under certain circumstances. Thus, for atmospheres represented by this case, the physical retrieval is unnecessary if fast productions are required. However, a significant difference between the statistical regression retrieval and the physical iteration retrieval could occur when the training data set used to generate the regression coefficients does not statistically represent the measured atmospheric state; the final retrieval is improved through physical iterations of radiative transfer computation comparison.

Comparison of both the water vapor mixing ratio and relative humidity between the LASE and the NAST-I final physical retrieval are shown in Fig. 11. The LASE relative humidity is computed from the LASE mixing ratio by use of coincident NAST-I temperatures. The higher vertical resolution water vapor mixing ratios measured by the active remote sensor LASE onboard the DC-8 were taken almost at the same time and at the same location as the NAST-I measurements. The discrepancy is due to different vertical resolutions (approximately

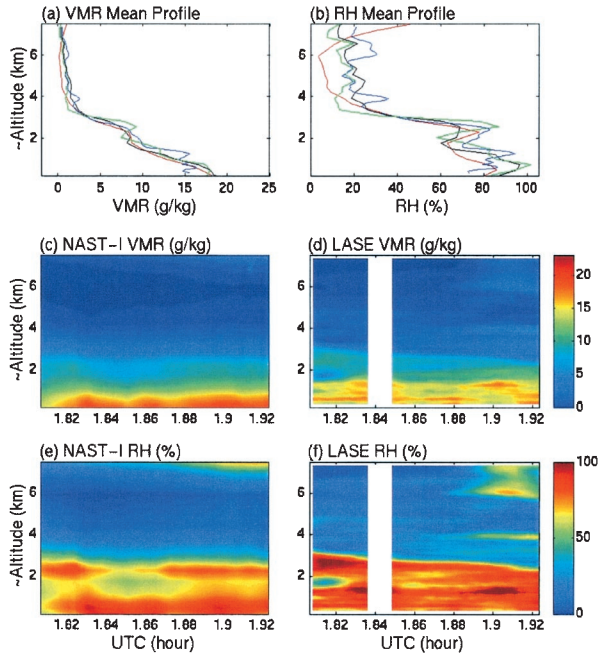

Fig. 11. Water vapor mixing ratio and relative humidity comparisons between NAST-I and LASE. (a) Mean profiles were produced from (c) NAST-I data (red) and (d) LASE data (blue), respectively, and the means in (b) were produced from (e) NAST-I data (red) and (f) LASE data (blue), respectively. In addition, the radiosonde (black) and Raman lidar (green) are also plotted for comparison (see text).

1 km for NAST-I and 0.33 km for LASE) and within expected error sources (e.g., NAST-I measurement and retrieval uncertainty). In addition, the mean water vapor profile from the ground observation of Raman lidar during this period is also plotted; the relative humidity is computed by use of radiosonde temperatures. Overall, good agreement between these sensors is illustrated, which validates the accuracy of NAST-I measurements and the retrieval algorithm.

This same data set is also displayed for horizontal levels showing that fine-scale horizontal features are retrievable from the NAST-I radiance observations. The skin temperature distribution, shown in Fig. 12(a) and for the time associated with the vertical distribution of Fig. 6 (or Fig. 9), indicates relatively warmer water skin temperature than land (island) skin temperature as expected for the local night observation time. The emissivity at the 8.6-μm region only varies approximately 2.0% as shown in Fig. 12(b). Samples of NAST-I geophysical products, horizontal distributions of temperature and relative humidity shown in Fig. 12(c) (or at any pressure level), together with the vertical distribution (Fig. 9) from nadir observations (or at any other viewing angle) along the flight track, clearly reveal the atmospheric state three dimensionality.

6. Summary

The algorithm used for temperature and moisture retrieval from NAST-I radiance observations has

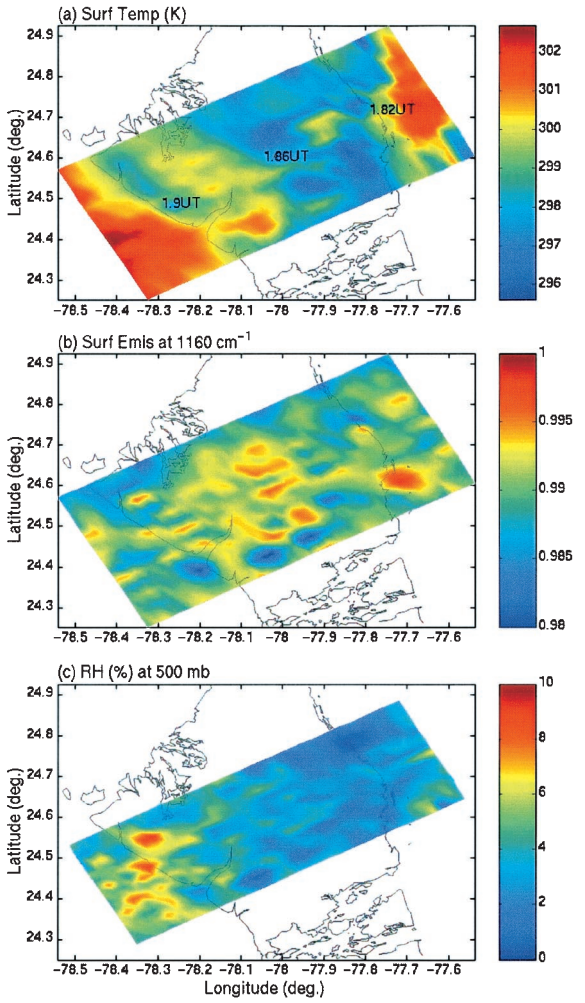

Fig. 12. Same data set as shown in Fig. 6 displayed in select horizontal levels: (a) skin temperature, (b) surface emissivity, (c) relative humidity at 500 mbars (see text).

been developed, validated, and demonstrated. Detailed statistical regression analyses were performed to better understand the effects of noise in the spectral radiance on retrieval accuracy, and thus in the selection of an optimal EOF number for a statistical regression retrieval process. An optimal number of EOFs can be determined by retrieval simulation with an accurate estimate of instrument noise. This can also be determined by minimization of the difference between observed radiance spectra and radiance spectra calculated from the retrievals of radiance observations. This latter method does not require *a priori* knowledge of the instrument and forward model noise level. The optimal EOF number determines the retrieval error and the vertical resolution associated with the noise level.

A nonlinear physical iteration retrieval algorithm has also been developed, validated, and demonstrated. The result of physical iteration is used to validate the accuracy of the regression retrieval used as a first guess. The analyses and retrievals from many field campaigns with varied meteorological

conditions (not presented here) illustrate the integrity of this retrieval approach. Retrieval samples of geophysical products from 13–14 September 1998 are presented here to demonstrate the capability of the NAST-I sensor to provide local mesoscale Earth science observations. The results demonstrate that accurate retrievals can be achieved without resorting to radiosonde tuning (i.e., radiance bias correction), an important feature of state-of-the-art remote sensing for near-nadir-viewing observation systems.

The NAST-I program is supported by the NPOESS Integrated Program Office (IPO) under contract NEEA5100-0-00188. The authors express sincere thanks to the NAST-I team members from various organizations. The authors also acknowledge support from the NASA Langley Research Center. LASE data and Raman lidar data were kindly provided by Edward V. Browell and Richard A. Ferrare of the NASA Langley Research Center.

References

1. D. Q. Wark and H. E. Fleming, "Indirect measurements of atmospheric temperature profiles from satellite: I. Introduction," Mon. Weather Rev. **94,** 351–362 (1966).
2. W. L. Smith and H. M. Woolf, "The use of eigenvectors of statistical co-variance matrices for interpreting satellite sounding radiometer observations," J. Atmos. Sci. **33,** 1127–1140 (1976).
3. W. W. McMillan, L. L. Strow, W. L. Smith, H. E. Revercomb, H. L. Huang, A. M. Thompson, D. P. McNamara, and W. F. Ryan, "Remote sensing of carbon monoxide over the continental United States on September 12–23, 1993," J. Geophys. Res. **102,** 10695–10709 (1997).
4. W. L. Smith, A. M. Larar, D. K. Zhou, C. A. Sisko, J. Li, B. Huang, H. B. Howell, H. E. Revercomb, D. Cousins, M. J. Gazarik, and D. Mooney, "NAST-I: results from revolutionary aircraft sounding spectrometer," in *Optical Spectroscopic Techniques and Instrumentation for Atmospheric and Space Research III*, A. M. Larar, ed., Proc. SPIE **3756,** 2–8 (1999).
5. W. L. Smith, D. K. Zhou, F. W. Harrison, H. E. Revercomb, A. M. Larar, A. H. Huang, and B. Huang, "Hyperspectral remote sensing of atmospheric profiles from satellites and aircraft," in *Hyperspectral Remote Sensing of the Land and Atmosphere*, W. L. Smith and Y. Yasuoka, eds., Proc. SPIE **4151,** 94–102 (2001).
6. S. E. Hannon, L. L. Strow, and W. W. McMillan, "Atmospheric infrared fast transmittance models: a comparison of two approaches," in *Optical Spectroscopic Techniques and Instrumentation for Atmospheric and Space Research II*, P. B. Hays and J. Wang, eds., Proc. SPIE **2830,** 94–105 (1996).
7. M. T. Chahine, H. Aumann, M. Goldberg, L. McMillin, P. Rosenkranz, D. Staelin, L. Strow, and J. Susskind, "AIRS-team retrieval for core products and geophysical parameters," *Algorithm Theoretical Basis Document*, JPL D-17006, M. Gunson, ed. (Jet Propulsion Laboratory, National Aeronautics and Space Administration, Pasadena, Calif., 2001).
8. D. K. Zhou, W. L. Smith, and A. M. Larar, "Temperature and moisture retrieval algorithm development for the NAST interferometer," in *Proceedings, International Radiation Symposium 2000: Current Problems in Atmospheric Radiation*, W. L. Smith, and Y. M. Timofeyev, eds. (Deepak Publishing, Hampton, Va., 2001), pp. 847–850.
9. D. K. Zhou, W. L. Smith, and A. M. Larar, "Tropospheric ozone near-nadir-viewing IR spectral sensitivity and ozone measurements from NAST-I," in *Hyperspectral Remote Sensing of the Land and Atmosphere*, W. L. Smith, and Y. Yasuoka, eds., Proc. SPIE **4151,** 277–284 (2001).
10. D. Cousins and W. L. Smith, "National Polar-Orbiting Operational Environmental Satellite System (NPOESS) Airborne Sounder Testbed-Interferometer (NAST-I)," in *Application of Lidar to Current Atmospheric Topics II*, A. J. Sedlacek and K. W. Fischer, eds., Proc. SPIE **3127,** 323–331 (1997).
11. A. M. Larar, W. L. Smith, D. K. Zhou, E. V. Browell, R. A. Ferrare, H. E. Revercomb, and D. C. Tobin, "Spectral radiance validation studies using NAST-I and other independent measurement systems," in *Optical Spectroscopic Techniques, Remote Sensing, and Instrumentation for Atmospheric and Space Research IV*, A. M. Larar and M. G. Mlynczak, eds., Proc. SPIE **4485,** 81–90 (2002).
12. R. A. Ferrare, E. V. Browell, S. Ismail, W. L. Smith, W. Edwards, A. Moore, S. Kooi, V. Brackett, M. Clayton, S. Fastig, D. Harper, L. Petway, L. Mathews, D. Whiteman, F. J. Schmidlin, D. Lauritsen, and R. May, "LASE measurements of water vapor, aerosols, and clouds during CAMEX-3," in *Optical Remote Sensing of the Atmosphere, 1999, Postconference Digest* (Optical Society of America, Washington, D.C., 1999), pp. 114–116.
13. W. L. Smith (NASA Langley Research Center), G. E. Bingham, M. J. Gordon, G. W. Cantwell, D. K. Zhou, and H.-L. Huang, "AIRS cloud-cleaning using multi-spectral MODIS imagery," IEEE Trans. Geosci. Remote Sens., submitted for publication.
14. W. L. Smith, "An improved method for calculating tropospheric temperature and moisture from satellite radiometer measurements," Mon. Weather Rev. **96,** 387–396 (1968).
15. J. W. Salisbury and D. M. D'Aria, "Emissivity of terrestrial material in the 8–14 μm atmospheric window," Remote Sens. Environ. **42,** 83–106 (1992).
16. D. K. Zhou, W. L. Smith, and A. M. Larar, "Surface temperature and emissivity from airborne measurements of IR radiance spectra," Eos Trans. Am. Geophys. Union Fall Meet. Suppl. **82**(47), A21B–0063 (2001).
17. Courtesy of H. Woolf, Space Science and Engineering Center, University of Wisconsin–Madison, Madison, Wisconsin 53706, and F. Schmidlin, NASA Wallops Flight Facility, Wallops Island, Virginia.
18. J. Li, "Temperature and water vapor weighting functions from radiative transfer equation with surface emissivity and solar reflectivity," Adv. Atmos. Sci. **11,** 421–426 (1994).
19. X. L. Ma, T. J. Schmit, and W. L. Smith, "A nonlinear physical retrieval algorithm—its application to the GOES-8/9 sounder," J. Appl. Meteorol. **38,** 501–513 (1999).
20. J. Li, W. W. Wolf, W. P. Menzel, W. Zhang, H. L. Huang, and T. H. Achtor, "Global soundings of the atmosphere from ATOVS measurements: the algorithm and validation," J. Appl. Meteorol. **39,** 1248–1268 (2000).
21. C. D. Rodgers, "Retrieval of atmospheric temperature and composition from remote measurements of thermal radiation," Rev. Geophys. Space Phys. **14,** 609–624 (1976).
22. J. R. Eyre, "Inversion of cloudy satellite sounding radiances by nonlinear optimal estimation. I: Theory and simulation for TOVS," Q. J. R. Meteorol. Soc. **42,** 1001–1026 (1989).
23. J. Susskind, J. Rosenfield, D. Reuter, and M. T. Chahine, "Remote sensing of weather and climate parameters from HIRS2/MSU on TIROS-N," J. Geophys. Res. **89,** 4677–4697 (1984).
24. C. M. Hayden, "GOES-VAS simultaneous temperature-moisture retrieval algorithm," J. Appl. Meteorol. **27,** 705–733 (1988).

25. W. L. Smith, H. M. Woolf, C. M. Hayden, and A. J. Schreiner, "The simultaneous export retrieval package," in *Technical Proceedings of the Second International TOVS Study Conference*, W. P. Menzel, ed. (Cooperative Institute for Meteorological Satellite Studies, University of Wisconsin–Madison, Madison, Wis., 1985), pp. 224–253.
26. J. Li and H. L. Huang, "Retrieval of atmospheric profiles from satellite sounder measurements by use of the discrepancy principle," Appl. Opt. **38,** 916–923 (1999).
27. V. A. Morozov, *Methods for Solving Incorrectly Posed Problems* (Springer-Verlag, New York, 1984).
28. M. F. Carfora, F. Esposito, and C. Serio, "Numerical methods for retrieving aerosol size distributions from optical measurements of solar radiation," J. Aerosol Sci. **29,** 1225–1236 (1998).